Materials Chemistry and Physics 320 (2024) 129400

Contents lists available at ScienceDirect

Materials Chemistry and Physics

journal homepage: www.elsevier.com/locate/matchemphys

Solid state synthesis, structural, DFT and spectroscopic analysis of $EuAl_3(BO_3)_4$

A.S. Oreshonkov [a,b,*], A.S. Aleksandrovsky [c,d], O.D. Chimitova [e], D.V. Pankin [f], Z.I. Popov [g,h], E. V. Sukhanova [g,i], M.S. Molokeev [j,k], S.V. Adichtchev [l], A.M. Pugachev [l], I.V. Nemtsev [a,m,n]

[a] Laboratory of Molecular Spectroscopy, Kirensky Institute of Physics, Federal Research Center KSC SB RAS, Krasnoyarsk, 660036, Russia
[b] School of Engineering and Construction, Siberian Federal University, Krasnoyarsk, 660041, Russia
[c] Laboratory of Coherent Optics, Kirensky Institute of Physics, Federal Research Center KSC SB RAS, Krasnoyarsk, 660036, Russia
[d] Institute of Nanotechnology, Spectroscopy and Quantum Chemistry, Siberian Federal University, Krasnoyarsk, 660041, Russia
[e] Laboratory of Oxide Systems, Baikal Institute of Nature Management, SB RAS, Ulan-Ude, 670047, Russia
[f] Center for Optical and Laser Materials Research, Saint-Petersburg State University, Saint-Petersburg, 199034, Russia
[g] Emanuel Institute of Biochemical Physics of Russian Academy of Sciences, Moscow, 119334, Russia
[h] Plekhanov Russian University of Economics, Moscow, 117997, Russia
[i] Moscow Institute of Physics and Technology, Dolgoprudny, 141700, Russia
[j] Laboratory of Crystal Physics, Kirensky Institute of Physics, Federal Research Center KSC SB RAS, Krasnoyarsk, 660036, Russia
[k] School of Engineering Physics and Radio Electronics, Siberian Federal University, Krasnoyarsk, 660041, Russia
[l] Institute of Automation and Electrometry, Russian Academy of Sciences, Novosibirsk, 630090, Russia
[m] Department of Molecular Electronics, Federal Research Center Krasnoyarsk Science Center of the Siberian Branch of the Russian Academy of Sciences, Krasnoyarsk, 660036, Russia
[n] Institute of Fundamental Biology and Biotechnology, Siberian Federal University, Krasnoyarsk, 660041, Russia

HIGHLIGHTS

- The synthesis of trigonal $EuAl_3(BO_3)_4$ powder using a multi-stage solid-state reaction method.
- Midgap states are attributed to the Eu^{3+} f-states, but no emphasized peaks are observed on the simulated absorbance spectra.
- The contribution of molecular groups and individual ions to the Raman spectrum is demonstrated.
- Ultranarrow $^5D_0 .\rightarrow {}^7F_0$ luminescent line serves as a monitor for limited number of structural defects in trigonal $EuAl_3(BO_3)_4$.

ARTICLE INFO

Keywords:
$EuAl_3(BO_3)_4$
Huntite
X-ray diffraction
SEM
DFT
Charge transfer
Raman
Infrared
Luminescence

ABSTRACT

Huntite-like borates are versatile and promising materials with wide range of applications in frequency conversion, UV light generation, lighting, displays, quantum information storage, and more, demonstrated by their various properties and uses in scientific research. In this work, $EuAl_3(BO_3)_4$ powder was prepared through multi-stage solid-state reaction method using high-purity starting reagents: Eu_2O_3, Al_2O_3 and H_3BO_3, considering a 20 wt% excess of H_3BO_3 to compensate for B_2O_3 volatilization. Obtained samples undergo several treatments at varying temperatures and their phase purity is subsequently verified through powder X-ray diffraction analysis. The scanning electron microscopy reveals that resulting $EuAl_3(BO_3)_4$ powder consists of granules exhibiting irregular morphologies with dimensions of 0.5–8 μm. The electronic band structure of $EuAl_3(BO_3)_4$, calculated using the GGA PBE method, reveals f-states of Eu near 4 eV. These states do not produce emphasized peaks on simulated absorbance spectra. Using of DFT + U for the f-states of Eu pushed up f-bands above 6 eV and the charge transfer from p-O to d-Eu was obtained (E_g^{direct} = 5.63 eV, $E_g^{indirect}$ = 5.37 eV using U_{eff} = 4 eV). The variation of U_{eff} has a weak influence on the position of the bottom of the conduction band. The experimental bandgaps of $EuAl_3(BO_3)_4$ crystalline powder, both direct and indirect, are found to be 3.96 and 3.67 eV, correspondingly. These values are lower than theoretical values what is associated with limitations of DFT calculations involving f electrons. The Raman spectrum of $EuAl_3(BO_3)_4$ powder is discussed, detailing the contributions of different ions to specific spectral bands. Investigation of high-resolution luminescence spectra shows

* Corresponding author. Kirensky Institute of Physics, Federal Research Center KSC SB RAS, Krasnoyarsk, 660036, Russia.
E-mail address: oreshonkov@iph.krasn.ru (A.S. Oreshonkov).

https://doi.org/10.1016/j.matchemphys.2024.129400
Received 2 November 2023; Received in revised form 29 February 2024; Accepted 30 April 2024
Available online 2 May 2024

the possibility to estimate the content of defects by the testing the violation of the prohibition of ultranarrow $^5D_0 \rightarrow {}^7F_0$ line that is forbidden in the ideal crystalline structure of trigonal $EuAl_3(BO_3)_4$.

1. Introduction

Huntite-like borates are regarded as promising materials for a broad spectrum of applications. In case of aluminum-containing compounds with the general formula $LnAl_3(BO_3)_4$ (Ln = lanthanides, Y), attention is paid to almost all compounds in this series. For example, the process of frequency conversion is important in various scientific and technological applications. The fourth harmonic generation of a frequency doubled Nd:YAG laser, from 532 to 266 nm, was carried out with $YAl_3(BO_3)_4$ crystal doubler in work of Yu et al. [1]. Thus, $YAl_3(BO_3)_4$ can be considered as a potential material for generation of UV light. At the same time, the Gd^{3+} doped $YAl_3(BO_3)_4$ is investigated as a new UV phosphor under excitation by VUV radiation. A strong emission line at 313 nm, resulting from the transitions between the $^6P_{7/2}$ and $^8S_{7/2}$ states of Gd^{3+} ions, was detected [2]. The $LnAl_3(BO_3)_4$ borates display growth in trigonal [3] and monoclinic structures. One of such examples can be seen for $SmAl_3(BO_3)_4$ [4]. $EuAl_3(BO_3)_4$ crystals containing coherent stacking sequences of three known polymorphs are suggested as the media for quantum information storage [5]. $GdAl_3(BO_3)_4$: Dy^{3+}, Eu^{3+} phosphor considered as an excellent choice for solid-state lighting and displays [6,7]. The $GdAl_3(BO_3)_4$:Cr^{3+} was characterized as highly efficient and thermally stable phosphor with a broad NIR emission band (FWHM of ~140 nm) in the spectral range of 650–1000 nm. This characteristic sets it apart and establishes its potential as an outstanding commercial phosphor for NIR pc-LEDs (phosphor-converted light-emitting diodes), particularly in applications such as plant lighting and food analysis [8]. In work of Ruggieri et *al* [9], it was shown that the addition of Eu^{3+} ions to the $TbAl_3(BO_3)_4$ matrix changes the emission color of media progressively from green to yellow, orange, and finally red. The (Er,Yb):$LuAl_3(BO_3)_4$ crystals have demonstrated their efficacy in diode-pumped lasing, particularly in the spectral region of 1.5–1.6 μm, which is considered safe for the human eye [10].

As it was previously shown in work of Oreshonkov et al. [11], the band gap value of $YAl_3(BO_3)_4$ should be not less then 5.1 eV and the charge transfer in this case associated with transitions from p electrons of O to d electrons of yttrium. It was presented in work of Ju et al. [12], that in Nd-doped $YAl_3(BO_3)_4$, trigonal and monoclinic $NdAl_3(BO_3)_4$, the occupied states appeared above Fermi level and these states related to f states. The suggested band gaps were found in range from 1.1 to 1.5 eV, while the transitions from the p-O to d-Nd states were observed to start from 5.5 eV, however, no calculated absorption spectra were shown. It is clearly evident that there is a significant data gap for other members of this crystal family. This issue can be attributed to the difficulties in accounting for f-electron shells, the high demand for computational resources and absence of experimental data. All these factors make it difficult to understand the electronic structure of the discussed compounds.

The triangular coordination of boron (BO_3) in huntite-like compounds can be easily confirmed using vibrational spectroscopy. However, the spectrum below 500 cm^{-1} corresponds to complex forms of vibrations of other structural units (or to their mixed vibrations) and may cause difficulties for interpretation [13]. In such cases, for example, factor group analysis can be used [14]. Nevertheless, sometimes authors used the word 'probably' [15]. In such cases, it is possible to perform calculations of phonon density of states [11,16–20], however, we have not found an example of such a calculation for huntite-like borates.

The spectral energy distribution of the luminescence spectrum is greatly influenced by the site symmetry of the Eu^{3+}. For example, in Eu^{3+}-activated $YAl_3(BO_3)_3$, dominant lines at 614 nm and 619 nm correspond to the $5D_0 \rightarrow 7F_2$ transition, while two fainter lines at 592 nm and 596 nm are attributed to the $5D_0 \rightarrow 7F_1$ transition [21]. As discussed in work of Blasse et al. [21], if the local environment of Eu^{3+} is a trigonal prism with D_{3h} symmetry, the number of lines in the transitions $5D_0 \rightarrow 7F_2$ should be equal to one. However, since two lines are observed, the site symmetry must be D_3. That is in agreement with defined site symmetry of rare-earth ions in $YAl_3(BO_3)_4$ matrix [11]. A detailed analysis of absorption spectrum of Eu^{3+}-doped $GdAl_3(BO_3)_4$ is given in work of Gorller-Walrand et al. [22]. The absorption, fluorescence and magnetic circular dichroism spectra of $YAl_3(BO_3)_4/Eu^{3+}$ crystal are discussed by Gorller-Walrand et al. too [23].

Experimental $5D_0 \rightarrow 7F_1$, $5D_0 \rightarrow 7F_2$ and $5D_0 \rightarrow 7F_4$ luminescent bands for $EuAl_3(BO_3)_4$ were shown in work of Malashkevich et al. [24], however, some remarks about $5D_0 \rightarrow 7F_0$ need to be voiced. In work of Tanabe et al. [25], fluorescence spectra of crystalline and amorphous samples were presented. Only the presence of $5D_0 \rightarrow 7F_1$ and $5D_0 \rightarrow 7F_2$ transitions was observed in the range from 560 to 650 nm for single crystal sample. A wide spectral band from 575 to 580 nm appeared in spectrum of amorphous sample and it was classified as $5D_0 \rightarrow 7F_0$. The dip in the spectra around 580 nm is observed in both the works of Malashkevich et al. [24] and Tanabe et al. [25]. However, as it was demonstrated in the article by Atuchin et al. [26], the $^5D_0 \rightarrow {}^7F_0$ transition in Eu^{3+} ions of $Eu_2(MoO_4)_3$ is manifested like the ultranarrow band around 580 nm. Thus, it can be assumed that in discussed above works, the ultranarrow $5D_0 \rightarrow 7F_0$ transition was not detected. In addition, it can also be said that $5D_0 \rightarrow 7F_0$ line of Eu^{3+} ion is traditionally used as the probe of site symmetry (see, for example [27]).

In the present paper we report on solid state synthesis of $EuAl_3(BO_3)_4$ powder. Investigation addresses its absorption spectrum and the results of electronic structure calculations. The features of luminescence spectrum of powder sample are discussed. We focus onto the investigation of the formation of the optical bandgap, comparison of absorption spectrum with DFT simulation and on the investigation of the luminescence in the vicinity of $^5D_0 \rightarrow {}^7F_0$ that is forbidden in ideal trigonal crystalline lattice, in order to examine the possibility of monitoring the content of defect sites occupied by Eu ion. Phonon density of states and analysis of atomic displacements were used to shown impact of certain ions and structural units on Raman spectrum.

2. Experimental and calculation methods

2.1. Synthesis

The samples were prepared by solid state reactions using high purity starting reagents (Red Chemist, Ltd., Russia): Eu_2O_3 (99.99 %), Al_2O_3 (99.99 %) and H_3BO_3 (99.99 %). The samples were synthesized by the traditional solid-state reaction method. Stoichiometric amounts of the raw materials were weighed according to the formula of $EuAl_3(BO_3)_4$, except a 20 wt% excess of H_3BO_3 was added to compensate for the volatilization of B_2O_3 during calcining. The chemicals were mixed thoroughly by grinding in an agate mortar and then put into a platinum crucible and heated up to 300 °C for 10 h in a muffle furnace. After being reground, the powder mixtures were sintered at 600 °C during 24 h. Further on, three 48 h treatments with intermediate grinding were performed at 900, 1000 and 1160 °C, respectively. Powder X-ray diffraction data were recorded by a D8 ADVANCE Bruker AXS diffractometer [28] (Vantec-1 detector) at room temperature using CuK_α radiation and scanning from $2\theta = 8°$–$100°$ in increments of 0.02° and a counting time of 0.1 s/step. Phase purity was verified by powder X-ray diffraction (XRD).

2.2. Powder X-ray diffraction

The powder diffraction data of $EuAl_3(BO_3)_4$ for Rietveld analysis was collected at room temperature with a Bruker D8 ADVANCE powder diffractometer (Cu-Kα radiation) and linear VANTEC detector. The step size of 2θ was 0.023°, and the counting time was 2 s per step.

2.3. Scanning electron microscopy

To study in a scanning electron microscope, the powder was mounted to a double-sided electrically conductive carbon tape for electron microscopy (TedPella, USA). Taking into account the dialectical nature of the sample, it was deposited with platinum in the EM ACE200 metal coater system (Leica, Vienna, Austria) at 25 mA for 60 s. The scanning electron microscopy (SEM) was carried out with a high-resolution scanning electron microscope FE-SEM S-5500 (Hitachi, Japan) at an accelerating voltage of 3 kV.

2.4. Density functional theory calculations

The electronic structure calculations were performed within the framework of density functional theory (DFT) [29,30] implemented in VASP program package [31–33]. The Perdew, Burke and Ernzerhof (PBE) exchange-correlation functional was used [34]. The projector-augmented wave (PAW) method based pseudopotentials [35] were applied in plane wave basis with the energy cutoff of 520 eV. For Eu, Al, B and O the pseudopotentials with 17, 3, 3 and 6 outer electrons were treated as valence electrons. The first Brillouin zone was sampled to 4 × 4 × 4 k-points according to Γ-centered mesh [36]. We use the DFT + U formalism in the Dudarev approach [37] for the 4f orbital of Eu with U_{eff} = 5.4 eV [38] and U_{eff} = 4 eV [39]. For atomic structure visualization we used VESTA 3 [40] software.

The CASTEP [41] code was used for lattice dynamics simulation. Wavenumber values closest to experimental ones were obtained using local density approximation [42] based on the Perdew and Zunger parametrization [43] of the numerical results of Ceperley and Alder [44]. Structural parameters were relaxed until the maximum forces and stress were less than 0.01 eV/Å and 0.02 GPa, respectively. Norm-conserving pseudopotentials generated on the fly (OTFG norm conserving) and a plane-wave cutoff of 1080 eV were used. The reciprocal space of the $EuAl_3(BO_3)_4$ primitive cell was sampled using a 4 × 4 × 4 Monkhorst–Pack k-mesh.

2.5. UV spectroscopy

The precision spectrophotometer Lambda1050 (PerkinElmer) was used to obtain the diffuse reflectance spectrum. The spectrum was obtained in the 190–850 nm region with the aid of R6872 PMT detector and integration sphere accessory which size was 150 mm. The scanning speed was 1 nm/s and the scanning step was 2 nm. The 0 % and 100 % calibrations were performed before measurement. The Spectralon White standard sample was used as the reference sample. On the basis of obtained spectrum, the Kubelka-Munk function was calculated. The band gap energy was determined from the Tauc plots in cases of direct and indirect allowed transitions [45].

2.6. Raman and luminescence

Raman light scattering spectra were obtained at room temperature in a backscattering geometry in the frequency range of 80–1400 cm^{-1} using a Fourier spectrometer Vertex 80 with FT-Raman R100/R RAM II. The excitation wavelength was 1064 nm and a power of 100 mV. The spectral resolution was about 2 cm^{-1}. Luminescence spectra were measured at room temperature on a TriVista 777 spectrometer (Princeton Instruments, USA) in a backscattering geometry. The spectra were recorded in the wavelength range from 535 nm to 720 nm. The spectral resolution was ~2 cm^{-1}. The 532.1 nm line of a Millennia laser (Spectra-Physics, USA) was used for excitation.

3. Results and discussion

The scanning electron microscopy (SEM) image of $EuAl_3(BO_3)_4$ powder shown in Fig. 1(a). Obtained granules have an irregular shape and their size varies from 0.5 to 8 μm. The composition of the obtained sample is examined using Energy-dispersive X-Ray spectroscopy (EDX). The extracted Eu/(Eu + Al) and B/(B + O) ratios agree with the chemical formula. The presence of peak related to Si (SiO_2) is associated with the sample grinding procedure in an agate mortar (SiO_2) [11]. The presence of a peak associated with carbon in spectrum is attributed to the use of a carbon conductive double-coated tape for sample mounting.

Experimental and calculated X-ray patterns, along with their comparison, are illustrated in Fig. 1(b). The calculated pattern was derived from the actual crystal structure of $EuAl_3(BO_4)_3$, which is isostructural to $ErAl_3(BO_4)_3$ [46], and is represented by the black line. The experimental pattern is shown as red points, while the difference between them is indicated by the gray line. Therefore, this structure was taken as starting model for Rietveld refinement which was performed using TOPAS 4.2 [47]. Site of Er ion was replaced by Eu ion and crystal structure of $EuAl_3(BO_3)_4$ is shown in Fig. 2. Refinement was stable and gave low R-factors (Table S1). Obtained lattice parameters are a = 9.3075 Å and c = 7.2764 Å. Coordinates of atoms and main bond lengths are in Table 1 and Table S2, respectively. The crystallographic data are deposited in Cambridge Crystallographic Data Centre (CCDC # 2302968). The data can be downloaded from the site (www.ccdc.cam.ac.uk/data_request/cif).

Calculated electronic band structure of $EuAl_3(BO_3)_4$ by GGA PBE method presented in Fig. 3. When using this method, the f-states of Eu is appeared on the top of valence bands and bottom of conductance bands near 4 eV. Despite to the presence of f-states of Eu at 4 eV we have no see emphasized peaks attributed to these states on simulated absorbance spectra (see Fig. 4). The absence of significant differences in the spectra obtained for different crystallographic directions indicates isotropic absorption in all directions. The DFT + U method can be applied to improve the description of systems with strongly correlated f electrons.

The analysis of calculated spectra in Fig. 4 indicates that the 4–6 eV range must be composed by the contribution from transitions between f electron levels of Eu ion at the top of valence band and excited f levels seen in the region of 4 eV in Fig. 3. These transitions are prohibited in dipole-dipole approximation for the free ion but can gain transition probability due to admixture of d orbitals by crystal field of D_3 symmetry. Calculated spectra are consistent with bandgap above 6 eV, however, part of that calculated spectrum in the range 4–6 eV can be pronounced in the experiment like, e. g., indirect bandgap approximately 4.5 eV.

The values for the Hubbard Coulomb repulsion parameter U for f electrons of Eu atoms were 4 eV and 5.4 eV, respectively. Results of using of PBE + U approach are shown in Fig. 5. Under U_{eff} = 5.4 the f-states of Eu pushed up from conductance band and the U_{eff} = 4 indicates the appearance of f-states of Eu at the bottom of conductance bands. For U_{eff} = 4 eV direct band gap equals to 5.63 eV and indirect to 5.37 eV, for U_{eff} = 5.4 eV direct band gap value is 5.68 eV and indirect is 5.41 eV.

The surface states can affect the electronic structure of materials and midgap states can appears or band gap value can change due to dimensionality decreased [48]. Based on experimental measurement of $EuAl_3(BO_3)_4$ particles size which in the range from 0.5 to 8 μm one can proposed the influence of surface states on electronic structure as well as on optical spectra. To examine this assumption, we prepare single layered structure from $EuAl_3(BO_3)_4$ crystal as shown in Fig. 6 (a), and performed the electronic structure calculation. As the discussed structure represent the limiting case of the crystal structure both side of this slab covered by BO3 triangles and whole stoichiometry of such structure equals to $EuAl_3(BO_3)_8$.

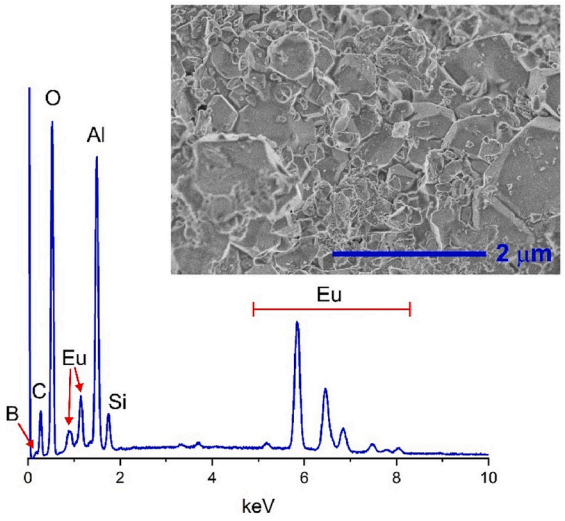

Composition of sample (at. %)

Eu	Al	B	O	Si
9.00	27.24	13.91	46.94	2.90

Eu/(Eu+Al) ratio	B/(B+O) ratio
0.25	0.25

(a)

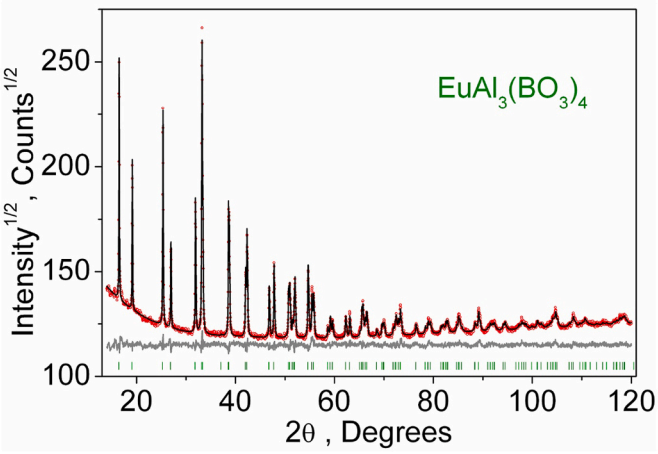

(b)

Fig. 1. (a) – scanning electron microscopy image, EDX spectrum and sample composition. (b) – difference Rietveld plot of $EuAl_3(BO_3)_4$ powder.

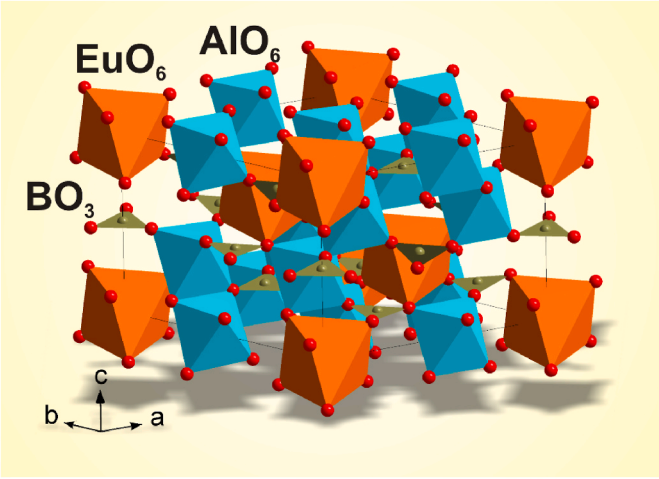

Fig. 2. Crystal structure of $EuAl_3(BO_3)_4$.

Table 1
Fractional atomic coordinates and isotropic displacement parameters (Å^2) of $EuAl_3(BO_3)_4$.

Atom	*x*	*y*	*z*	B_{iso}
Eu	0	0	0	0.40 (19)
Al	0.5532 (3)	0	0	0.30 (19)
B1	0	0	0.5	1.0 (3)
B2	0.434 (3)	0	0.5	1.0 (3)
O1	0.8561 (6)	0	0.5	0.8 (2)
O3	0.4426 (5)	0.148	0.515	0.8 (2)
O2	0.5830 (15)	0	0.5	0.8 (2)

From band structure (see Fig. 6 (b)) one can see the appearance of f-states of Eu in the range from 2 to 4 eV upper from Fermi level. The O p-states under Fermi level can be due to abundance of oxygen in slab structure.

The experimental direct and indirect electronic bandgaps in $EuAl_3(BO_3)_4$ crystalline powder can be found from Fig. 7 [49]. Indirect bandgap is found to be 3.67 eV while direct bandgap equals to 3.96 eV. These values are lower than those theoretically simulated with the help of PBE; the deficiency of DFT calculations with f electrons involved is rather well-known, though in case of Gd ion with half-filled f shell the error is expected to be absent, as recently was demonstrated, e.g., in

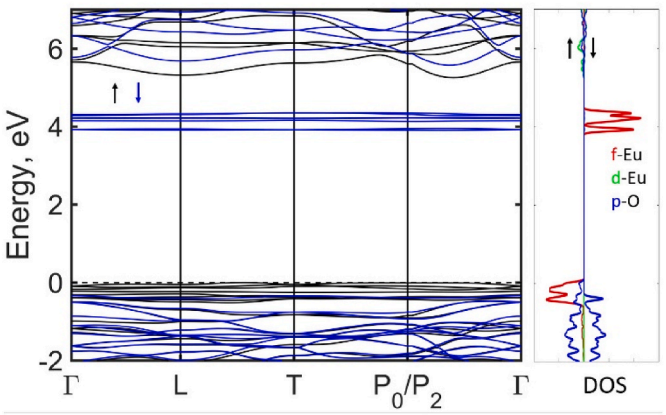

Fig. 3. Band structure and DOS of $EuAl_3(BO_3)_4$ simulated by GGA PBE.

work of Abulkhaev et al. [50] where meta-GGA RSCAN functional was used.

The Raman spectrum of the $EuAl_3(BO_3)_4$ powder obtained with a 1064-nm excitation shown in Fig. 8. Vertical ticks correspond to the calculated wavenumbers for the Raman-active vibrations. Total and partial phonon density of states (DOS) for $EuAl_3(BO_3)_4$ are shown in Fig. 9.

Unsurprisingly, the movements of the heavier Eu ions, as shown in Fig. 9 (a), contribute to the low wavenumber spectral band in the Raman spectrum. Contribution of aluminum to phonon DOS is significant from 200 to 605 cm^{-1}. The displacements of boron ions contribute significantly between 1250 and 1360 cm^{-1}. However, peaks corresponding to boron are also observed between 200 and 770 cm^{-1}. The calculation of partial phonon DOS has revealed that the O ions actively contribute to vibrations across the whole spectrum. Partial phonon density of states for crystallography independent boron and oxygen ions presented in Fig. 9 (b). From this figure we can conclude that spectral peak at 1340 cm^{-1} in Fig. 8 is a B2–O3 vibration in $B2O_3$ triangle, while broad band from 1250 to 1320 cm^{-1} is a B–O vibrations in $B1O_3$ and $B2O_3$. Strong band at 1020 cm^{-1} in Raman spectrum is a vibration of O2 and O3 ions in $B2O_3$ as a $\nu 1$ symmetric stretching vibration [51]. Medium Raman peak at 762 cm^{-1} and weak peak at 700 cm^{-1} are a ν_2-like vibrations of $B2O_3$ as shown in Fig. 10 (a). Weak band at 669 cm^{-1} related to $\nu 4$ BO_3 vibrational mode, see Fig. 10 (b). The weak band at 605 cm^{-1} is a ν_4 vibration of BO_3 with small translations of Al ions. Weak band at 521 cm^{-1} is an asymmetric O–Al–O stretching as shown in Fig. 10 (c). Strong band at 402 cm^{-1} (Fig. 10 (d)) and medium peak at 335 cm^{-1} are deformational vibrations of AlO_6 octahedra. According to Fig. 9 (a) and

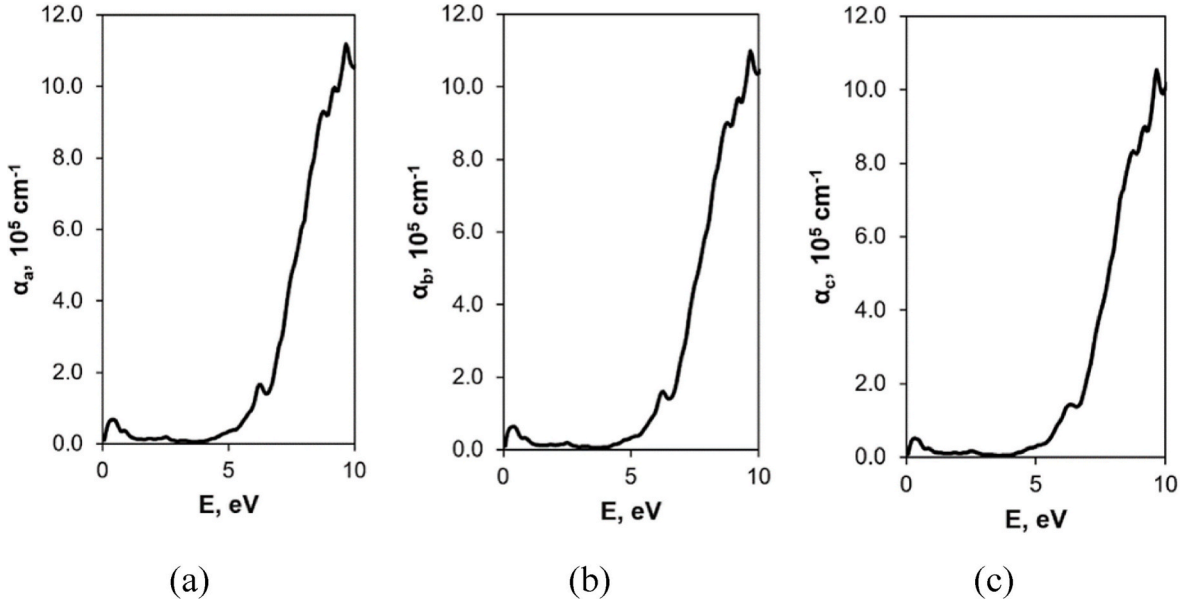

Fig. 4. Absorption spectra of $EuAl_3(BO_3)_4$ crystal simulated by GGA PBE for a) a, b) b, and c) c directions of the crystal structure.

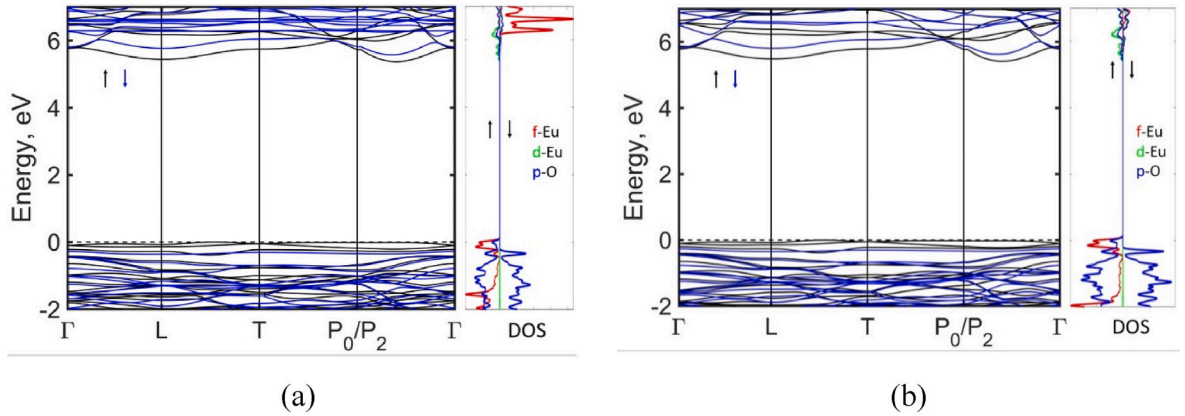

Fig. 5. Band structure and DOS of $EuAl_3(BO_3)_4$ simulated by PBE + U with U_{eff} = 4 eV (a) and U_{eff} = 5.4 eV.

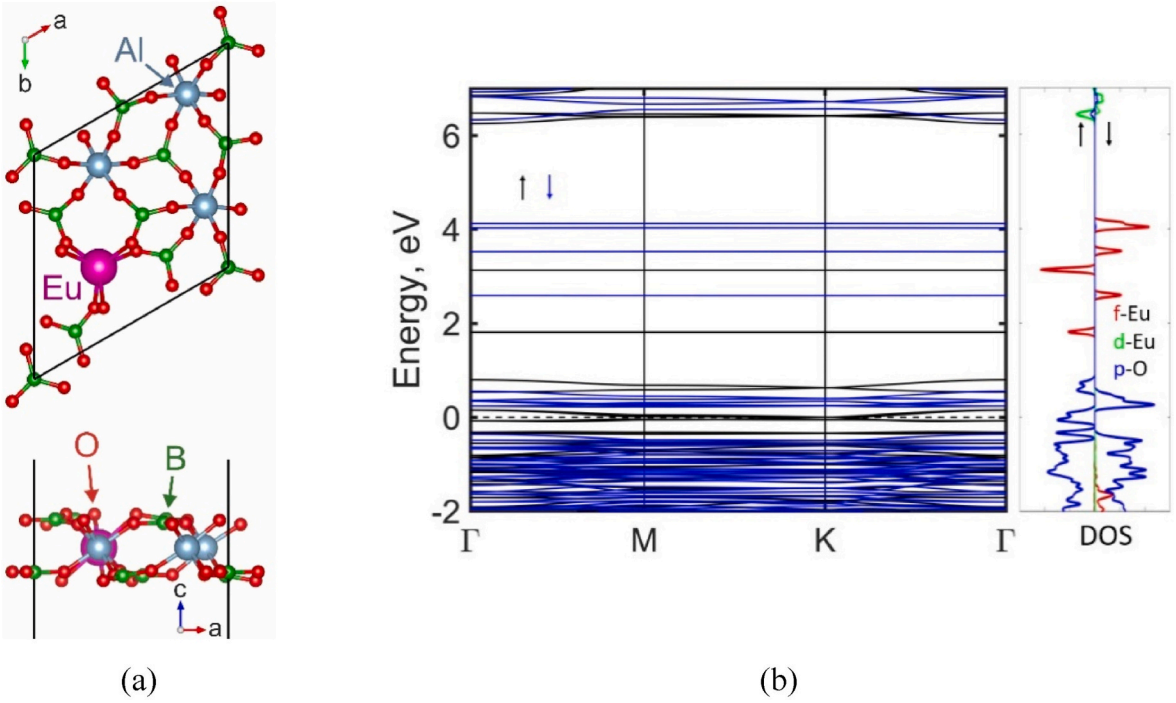

Fig. 6. Calculation of the band structure of the $EuAl_3(BO_3)_8$ slab. (a) Surface structure, (b) band structure.

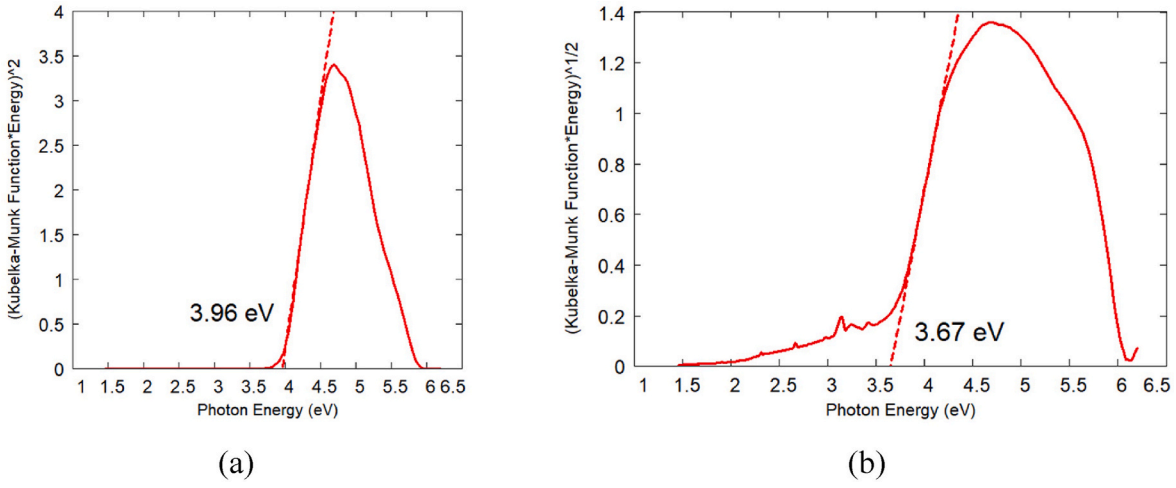

Fig. 7. Kubelka-Munk function and band gap determination for direct (a) and indirect (b) transitions in $EuAl_3(BO_3)_4$.

(b), strong band at 298 cm^{-1} in Fig. 8 is a translation of Al ions combined with movements of O3 ions as shown in Fig. 10 (e). Medium band at 258 cm^{-1} can be interpreted as a combination of $B1O_3$ translation in plane of boron triangle and translation of $B2O_3$ as shown in Fig. 10 (f). According to Fig. 9 (b), a band at 218 cm^{-1} in Raman spectrum associated with movements of oxygen with small contribution of boron and aluminum atoms.

Studies of the luminescence in many cases can be the source of information on the structure of the materials, allowing the possibilities to monitor certain structural features.

Luminescence spectrum of $EuAl_3(BO_3)_4$ powder excited at 532 nm is presented in Fig. 11. The excitation at the wavelength quoted above is performed via non-resonant population of $^5D_1$ level. Approximately 1 % of ions excited to $^5D_1$ state experience radiative decay to ^7F_J states, as shown in Fig. 11. The peak belonging to $^5D_1 \rightarrow {}^7F_1$ transition maximizes at 536 nm, and that belonging to $^5D_1 \rightarrow {}^7F_2$ transition maximizes at 554 nm. The rest of $^5D_1$ population nonradiatively decays to of $^5D_0$ state that, in its turn, experiences radiative decay to ^7F_J states. Observed luminescence pattern is in general consistent with local symmetry of Eu^{3+} ion within the crystal structure of trigonal huntite that is well-established to be D_3. In the particular, $^5D_0 \rightarrow {}^7F_1$ and $^5D_0 \rightarrow {}^7F_2$ bands contain two distinct crystal-field-split components [21] while $^5D_0 \rightarrow {}^7F_4$ band contains four crystal-field-split components. The $^5D_0 \rightarrow {}^7F_3$ is very weak that produced minor incorrectness in its assignment in Ref. [52]. In our spectrum, $^5D_0 \rightarrow {}^7F_3$ band peaks at 654.5 nm and contains four components, too, as is expected for D_3 local symmetry. The $^5D_0 \rightarrow {}^7F_4$ band peaks at 699 nm and contains six components, in accordance with D_3 local symmetry, too.

Let us examine the luminescence spectrum of $EuAl_3(BO_3)_4$ in the region of ultranarrow transition $^5D_0 \rightarrow {}^7F_0$ in more detail. It is well known that in D_3 local symmetry this transition remains to be strictly forbidden [21]. The Review by Binnemans [53] that includes analysis of

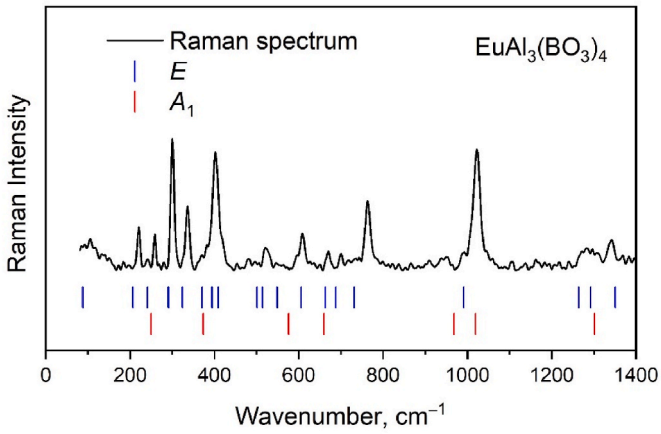

Fig. 8. Raman spectra of $EuAl_3(BO_3)_4$ at three different excitation wavelengths. Positions of vertical ticks corresponds to calculated wavenumbers.

spectra with this transition, does not report a single example when this transition is observed in a simple case of homovalent substitution by Eu^{3+} of sites with local symmetry other than C_n, C_s or C_{nv}. On the other hand, numerous examples can be provided of hetrovalent substitution of D_n sites by Eu^{3+} ion when $^5D_0 \rightarrow {}^7F_0$ is observable, and these cases are explained by the presence of charge compensating defect in the vicinity of Eu^{3+} ion. Then, local symmetry in these cases is formally D_n with account of first coordination sphere but is really lower than D_n with the account of neighboring defect. This is not the case of $EuAl_3(BO_3)_4$ where Eu^{3+} is the main host-forming ion occupying D_3 site, and no charge-compensating defects are expected. The luminescence spectrum of $EuAl_3(BO_3)_4$ in the vicinity of ultranarrow transition is presented in Fig. 12.

The broad structure in the range 575–579 nm in Fig. 12 indicated by asterisk must be ascribed to minor impurity indistinguishable by XRD, that is verified by the comparison with spectrum of monoclinic $Eu_2(MoO_4)_3$ [26] shown in magenta line. The lines of minor amplitude in the vicinity of 585 nm noticeably differ from neighboring spectral structures that must be assigned to the $^5D_1 \rightarrow {}^7F_3$ transition. This weak solitary line around 580 nm must be associated with the possible position of $^5D_0 \rightarrow {}^7F_0$ transition that is forbidden for Eu^{3+} ions in D_3 site of $EuAl_3(BO_3)_4$ huntite-like structure [21]. The lift of the prohibition for J = 0 to J = 0 transitions is commonly associated with J mixing by crystal field or even by admixing of charge transfer state that is known to be noticeably strong in case of Eu^{3+}. Then, presence of weak $^5D_0 \rightarrow {}^7F_0$ line can be ascribed to presence of small amount of structural defects in the second or higher coordination spheres of Eu^{3+} ion. Partially, this mechanism is supported by the observation of broad band in the vicinity of $^5D_0 \rightarrow {}^7F_4$ lines that can be ascribed to the luminescence from anion vacancies in oxide crystals (see, e.g. Ref. [54]). One more factor that may produce the violation of prohibition for ultranarrow line in huntites is the possible domain structure known for this crystal. Recently large domains in a iron-containing huntite single crystal were visualized by XNCD [55]. Domains are known to exist in iron-free huntite crystals, too. Aside large domain structures, one can imagine existence of such defects of submicron scale in huntites. In this case, violation of D_3 local symmetry will happen at the domain walls, and spectroscopy of $^5D_0 \rightarrow {}^7F_0$ transition can be reliable means to monitor the presence of small-scale domains that cannot be monitored by any other means.

4. Conclusions

In this study, we synthesized huntite-like $EuAl_3(BO_3)_4$ borate powder using a traditional solid-state reaction method from high-purity starting materials (Eu_2O_3, Al_2O_3 and H_3BO_3), with a 20 wt% excess of H_3BO_3 for B_2O_3 volatilization compensation. SEM analysis revealed that the size of granules with irregular morphologies spanning 0.5 to 8 μm. The electronic structure calculations using PBE model showed that f-states of Eu^{3+} ion near 4 eV do not produce pronounced peaks in the absorbance spectra. Discrepancies between theoretical and experimental bandgaps highlighted the limitations of DFT calculations for f electrons in case of studied EuAl3$(BO_3)_4$. The contribution of individual ions to Raman spectrum was evaluated using calculations of the phonon density of states and analysis of atomic displacements. High-resolution luminescence spectra indicated the potential for defect estimation using the ultranarrow $5D_0 \rightarrow 7F_0$ line analysis.

CRediT authorship contribution statement

A.S. Oreshonkov: Conceptualization, Data curation, Formal analysis, Investigation, Methodology, Project administration, Software, Supervision, Validation, Visualization, Writing – original draft, Writing – review & editing. **A.S. Aleksandrovsky:** Investigation, Validation, Visualization, Writing – original draft, Writing – review & editing. **O.D. Chimitova:** Data curation, Resources, Validation, Writing – original draft, Writing – review & editing. **D.V. Pankin:** Data curation, Formal analysis, Investigation, Writing – original draft. **Z.I. Popov:** Data curation, Software, Validation, Visualization, Writing – original draft,

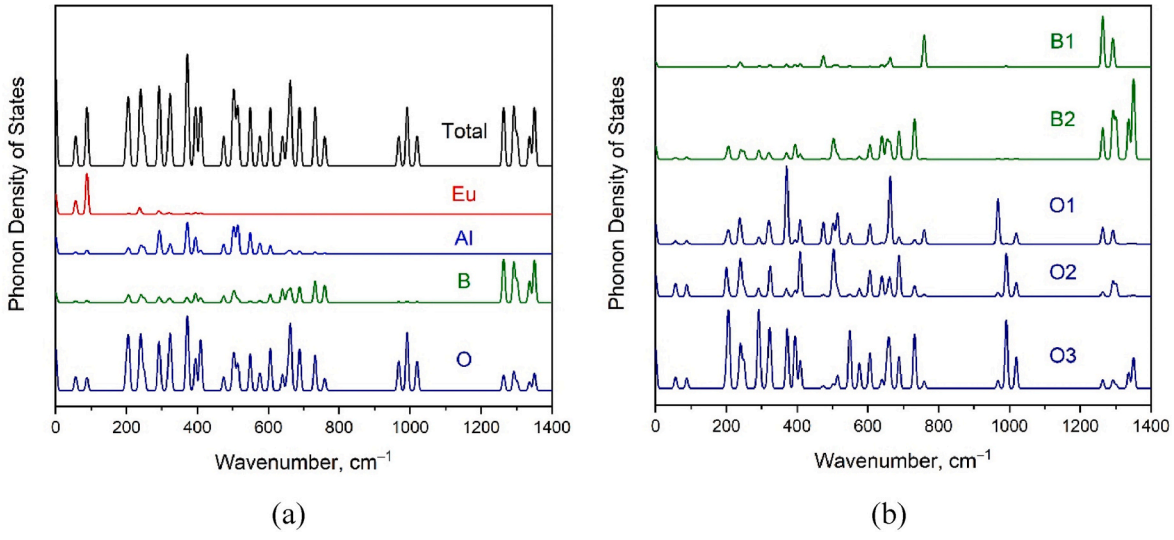

Fig. 9. Total and partial phonon density of states (a) including contribution of each B and O ions (b).

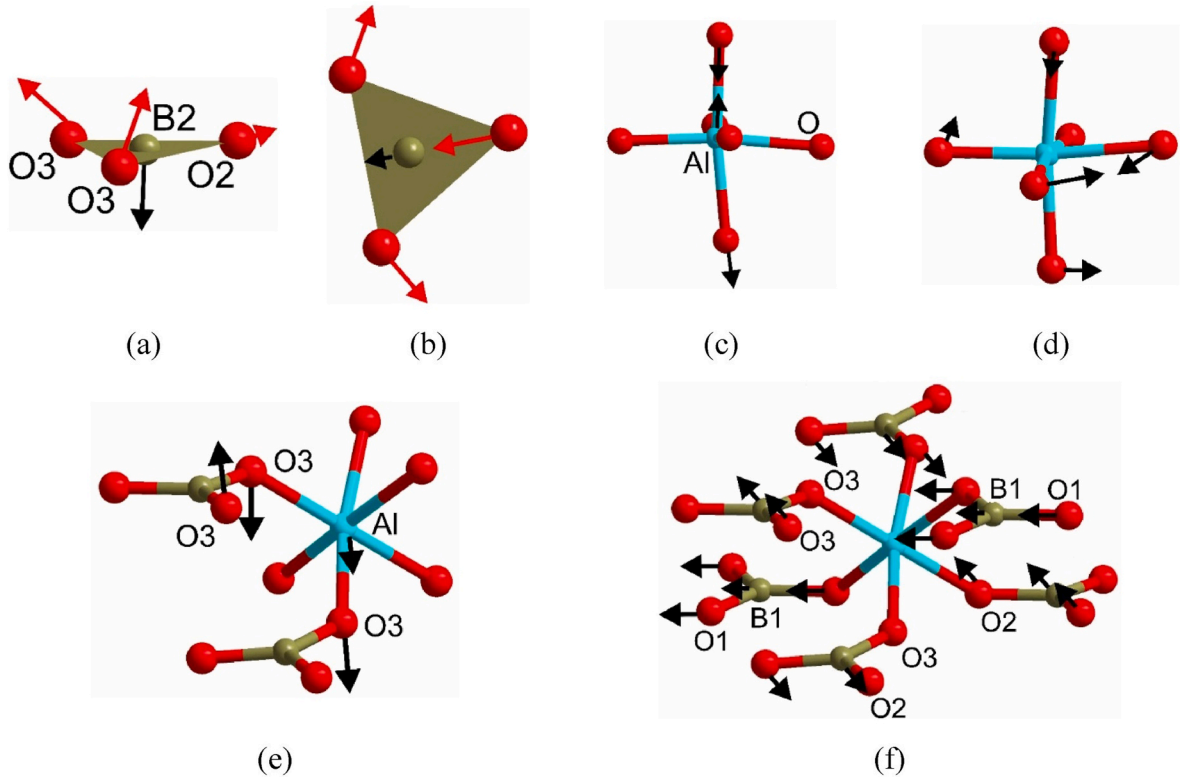

Fig. 10. Graphical representation of calculated vibrational modes: (a) E 731 cm^{-1}, (b) A_1 660 cm^{-1}, (c) E 513 cm^{-1}, (d) E 408 cm^{-1}, (e) E 291 cm^{-1}, (f) E 241 cm^{-1}.

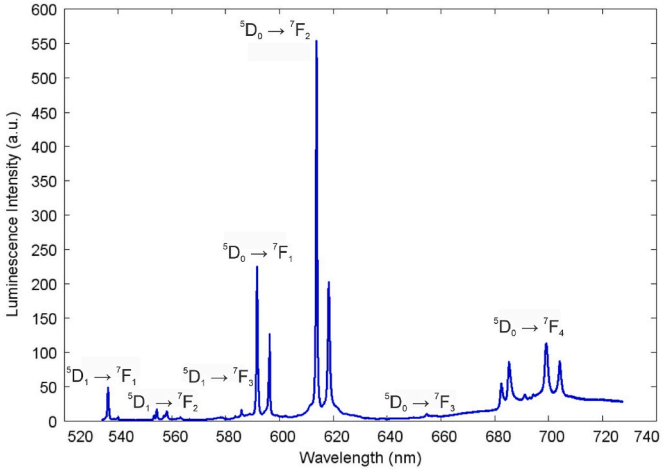

Fig. 11. Luminescence spectrum of $EuAl_3(BO_3)_4$ at room temperature excited at 532 nm.

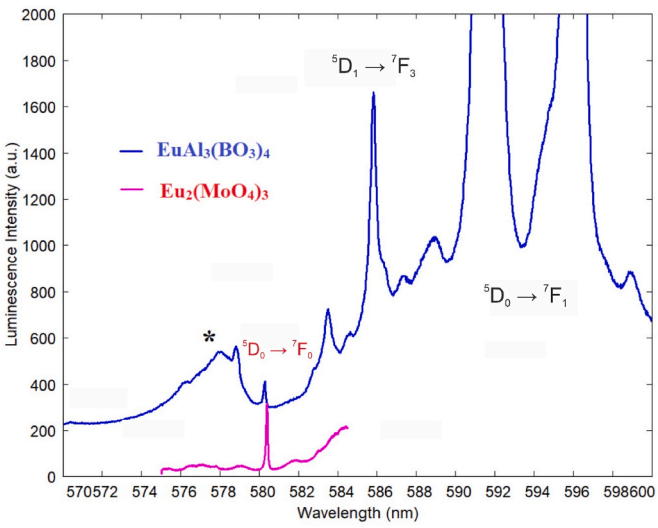

Fig. 12. Luminescence spectrum of $EuAl_3(BO_3)_4$ at 532 nm in the vicinity of ultranarrow $^5D_0 \rightarrow {}^7F_0$ transition.

Writing – review & editing. **E.V. Sukhanova:** Data curation, Software, Validation, Visualization, Writing – original draft. **M.S. Molokeev:** Data curation, Investigation, Validation, Visualization, Writing – original draft, Writing – review & editing. **S.V. Adichtchev:** Data curation, Investigation, Writing – original draft. **A.M. Pugachev:** Data curation, Investigation, Validation, Writing – original draft. **I.V. Nemtsev:** Data curation, Investigation, Validation, Visualization, Writing – original draft, Writing – review & editing.

Declaration of competing interest

The authors declare that they have no known competing financial interests or personal relationships that could have appeared to influence the work reported in this paper.

Data availability

Data will be made available on request.

Acknowledgments

The work was carried out within the state assignment No FWES-2024-0003 of Kirensky Institute of Physics. This work was partially supported by the state order of BINM SB RAS (0273-2021-0008). The

samples for this research were synthesized using equipment of the CCU BINM SB RAS. The reflectance spectrum was obtained at the Center for Optical and Laser Materials Research of Research park of St. Petersburg State University. The SEM measurements were performed at Krasnoyarsk Regional Center of Research Equipment of Federal Research Center « Krasnoyarsk Science Center SB RAS»

Appendix A. Supplementary data

Supplementary data to this article can be found online at https://doi.org/10.1016/j.matchemphys.2024.129400.

References

[1] X. Yu, Y. Yue, J. Yao, Z. Hu, YAl3(BO3)4: crystal growth and characterization, J. Cryst. Growth 312 (2010) 3029–3033, https://doi.org/10.1016/j.jcrysgro.2010.07.005.

[2] H. Yoshida, R. Yoshimatsu, S. Watanabe, K. Ogasawara, Optical transitions near the fundamental absorption edge and electronic structures of $YAl_3(BO_3)_4$:Gd^{3+}, Jpn. J. Appl. Phys. 45 (2006) 146–151, https://doi.org/10.1143/JJAP.45.146.

[3] A.D. Mills, Crystallographic data for new rare earth borate compounds, $RX_3(BO_3)_4$, Inorg. Chem. 1 (1962) 960–961, https://doi.org/10.1021/ic50004a063.

[4] A.S. Oreshonkov, N.P. Shestakov, M.S. Molokeev, A.S. Aleksandrovsky, I.A. Gudim, V.L. Temerov, S.V. Adichtchev, A.M. Pugachev, I.V. Nemtsev, E.I. Pogoreltsev, Y. G. Denisenko, Monoclinic $SmAl_3(BO_3)_4$: synthesis, structural and spectroscopic properties, Acta Crystallogr B Struct Sci Cryst Eng Mater 76 (2020) 654–660, https://doi.org/10.1107/S2052520620008781.

[5] Z.W. Riedel, B. Pan, T.J. Woods, D.P. Shoemaker, Stacking sequences of coherent $EuAl_3(BO_3)_4$ polymorphs define local Eu^{3+} symmetry and control access to quantum information storage, Cryst. Growth Des. 23 (2023) 6011–6018, https://doi.org/10.1021/acs.cgd.3c00566.

[6] O. Madkhali, Ü.H. Kaynar, S. Cam Kaynar, M. Ayvacikli, N. Can, Dy3+ and Eu3+ co-activated gadolinium aluminate borate phosphor: synthesis, enhanced luminescence, energy transfer and tunable color, Mater. Res. Bull. 164 (2023) 112282, https://doi.org/10.1016/j.materresbull.2023.112282.

[7] O. Madkhali, Ü.H. Kaynar, Y. Alajlani, M.B. Coban, J.G. Guinea, M. Ayvacikli, J. F. Pierson, N. Can, Structural and temperature dependence luminescence characteristics of RE (RE=Eu3+, Dy3+, Sm3+ and Tb3+) in the new gadolinium aluminate borate phosphor, Ceram. Int. 49 (2023) 19982–19995, https://doi.org/10.1016/j.ceramint.2023.03.120.

[8] D. Huang, H. Zhu, Z. Deng, H. Yang, J. Hu, S. Liang, D. Chen, E. Ma, W. Guo, A highly efficient and thermally stable broadband Cr^{3+} -activated double borate phosphor for near-infrared light-emitting diodes, J. Mater. Chem. C 9 (2021) 164–172, https://doi.org/10.1039/D0TC04803H.

[9] S. Ruggieri, L. Ceccon, M. Bettinelli, F. Piccinelli, Excited state dynamics of undoped and Eu^{3+} -doped $TbAl_3(BO_3)_4$ crystals, ECS J. Solid State Sci. Technol. 12 (2023) 066005, https://doi.org/10.1149/2162-8777/acde0d.

[10] V.V. Maltsev, D.A. Naprasnikov, A.D. Lyasnikov, N.I. Leonyuk, K.N. Gorbachenya, V.E. Kisel, A.S. Yasukevich, N.V. Kuleshov, Flux growth, thermal properties, and luminescence spectra of (Er,Yb,Lu)Al3(BO3)4 solid solutions, Inorg. Mater. 54 (2018) 826–830, https://doi.org/10.1134/S0020168518080125.

[11] A.S. Oreshonkov, E.M. Roginskii, N.P. Shestakov, I.A. Gudim, V.L. Temerov, I. V. Nemtsev, M.S. Molokeev, S.V. Adichtchev, A.M. Pugachev, Y.G. Denisenko, Structural, electronic and vibrational properties of YAl3(BO3)4, Materials 13 (2020) 545, https://doi.org/10.3390/ma13030545.

[12] M. Ju, G. Sun, X. Kuang, C. Lu, Y. Zhu, Y. Yeung, Theoretical investigation of the electronic structure and luminescence properties for $Nd_xY_{1-x}Al_3(BO_3)_4$ nonlinear laser crystal, J. Mater. Chem. C 5 (2017) 7174–7181, https://doi.org/10.1039/C7TC01911D.

[13] J.A. Campá, C. Cascales, E. Gutiérrez-Puebla, M.A. Monge, I. Rasines, C. Ruíz-Valero, Crystal structure, magnetic order, and vibrational behavior in iron rare-earth borates, Chem. Mater. 9 (1997) 237–240, https://doi.org/10.1021/cm960313m.

[14] E.Yu Borovikova, E.A. Dobretsova, K.N. Boldyrev, V.S. Kurazhkovskaya, V. V. Maltsev, N.I. Leonyuk, Vibrational spectra and factor group analysis of rare-earth chromium borates, RCr3(BO3)4, with R=La–Ho, Vib. Spectrosc. 68 (2013) 82–90, https://doi.org/10.1016/j.vibspec.2013.05.004.

[15] A. De Andrés, F. Agulló-Rueda, S. Taboada, C. Cascales, J. Campá, C. Ruiz-Valero, I. Rasines, Raman active phonons of RFe3(BO3)4, R=La or Nd, single crystals, J. Alloys Compd. 250 (1997) 396–399, https://doi.org/10.1016/S0925-8388(96)02556-X.

[16] V. Grossman, V. Atuchin, B.G. Bazarov, A. Aleksandrovsky, E. Eremin, A. Krylov, N. Kuratieva, J.G. Bazarova, N. Maximov, M. Molokeev, A. Oreshonkov, N. Pervukhina, N. Shestakov, Structural, spectroscopic, electric and magnetic properties of new trigonal K5FeHf(MoO4)6 orthomolybdate, Molecules 28 (2023) 1629, https://doi.org/10.3390/molecules28041629.

[17] E.V. Sukhanova, N.E. Sagatov, A.S. Oreshonkov, P.N. Gavryushkin, Z.I. Popov, Halogen-doped chevrel phase janus monolayers for photocatalytic water splitting, Nanomaterials 13 (2023) 368, https://doi.org/10.3390/nano13020368.

[18] A.N. Toksumakov, G.A. Ermolaev, A.S. Slavich, N.V. Doroshina, E.V. Sukhanova, D.I. Yakubovsky, A.V. Syuy, S.M. Novikov, R.I. Romanov, A.M. Markeev, A. S. Oreshonkov, D.M. Tsymbarenko, Z.I. Popov, D.G. Kvashnin, A.A. Vyshnevyy, A. V. Arsenin, D.A. Ghazaryan, V.S. Volkov, High-refractive index and mechanically cleavable non-van der Waals InGaS3, Npj 2D Mater Appl. 6 (2022) 85, https://doi.org/10.1038/s41699-022-00359-9.

[19] Y.G. Denisenko, V.V. Atuchin, M.S. Molokeev, A.E. Sedykh, N.A. Khritokhin, A. S. Aleksandrovsky, A.S. Oreshonkov, N.P. Shestakov, S.V. Adichtchev, A. M. Pugachev, E.I. Sal'nikova, O.V. Andreev, I.A. Razumkova, K. Müller-Buschbaum, Exploration of the crystal structure and thermal and spectroscopic properties of monoclinic praseodymium sulfate Pr2(SO4)3, Molecules 27 (2022) 3966, https://doi.org/10.3390/molecules27133966.

[20] A.S. Oreshonkov, E.V. Sukhanova, Z.I. Popov, Raman spectroscopy of janus MoSSe monolayer polymorph modifications using density functional theory, Materials 15 (2022) 3988, https://doi.org/10.3390/ma15113988.

[21] G. Blasse, A. Bril, W.C. Nieuwpoort, On the Eu^{3+} fluorescence in mixed metal oxides, J. Phys. Chem. Solid. 27 (1966) 1587–1592, https://doi.org/10.1016/0022-3697(66)90236-8.

[22] C. Gorller-Walrand, E. Huygen, K. Binnemans, L. Fluyt, Optical absorption spectra, crystal-field energy levels and intensities of Eu^{3+} in $GdAl_3(BO_3)_4$, J. Phys. Condens. Matter 6 (1994) 7797–7812, https://doi.org/10.1088/0953-8984/6/38/017.

[23] C. Görller-Walrand, P. Vandevelde, I. Hendrickx, P. Porcher, J.C. Krupa, G.S. D. King, Spectroscopic study and crystal field analysis of Eu3+ in the $YAl_3(BO_3)_4$ huntite matrix, Inorg. Chim. Acta. 143 (1988) 259–270, https://doi.org/10.1016/S0020-1693(00)83699-3.

[24] G.E. Malashkevich, V.N. Sigaev, N.V. Golubev, E.Kh Mamadzhanova, A. V. Danil'chik, V.Z. Zubelevich, E.V. Lutsenko, Rearrangement of optical centers and stimulated radiation of Eu^{3+} in polycrystalline huntite under optical and electron-beam excitation, Jetp Lett 92 (2010) 497–501, https://doi.org/10.1134/S0021364010200014.

[25] S. Tanabe, K. Hirao, N. Soga, T. Hanada, Preparation and fluorescence spectrum of amorphous huntite EuAl3(BO3)4, J. Solid State Chem. 97 (1992) 481–486, https://doi.org/10.1016/0022-4596(92)90058-4.

[26] V.V. Atuchin, A.S. Aleksandrovsky, O.D. Chimitova, T.A. Gavrilova, A.S. Krylov, M. S. Molokeev, A.S. Oreshonkov, B.G. Bazarov, J.G. Bazarova, Synthesis and spectroscopic properties of monoclinic α-$Eu_2(MoO_4)_3$, J. Phys. Chem. C 118 (2014) 15404–15411, https://doi.org/10.1021/jp5040739.

[27] I.V. Nikiforov, D.V. Deyneko, B.I. Lazoryak, Europium as a spectroscopic probe to determination site symmetry, 56–56, https://istina.msu.ru/publications/article/214249837/, 2019. (Accessed 26 October 2023).

[28] N.O. Azarapin, N.A. Khritokhin, V.V. Atuchin, A.A. Gubin, M.S. Molokeev, S. Mukherjee, O.V. Andreev, Kinetics and mechanism of BaLaCuS3 oxidation, Crystals 13 (2023) 903, https://doi.org/10.3390/cryst13060903.

[29] W. Kohn, L.J. Sham, Self-consistent equations including exchange and correlation effects, Phys. Rev. 140 (1965) A1133–A1138, https://doi.org/10.1103/PhysRev.140.A1133.

[30] P. Hohenberg, W. Kohn, Inhomogeneous electron gas, Phys. Rev. 136 (1964) B864–B871, https://doi.org/10.1103/PhysRev.136.B864.

[31] G. Kresse, J. Furthmüller, Efficient iterative schemes for ab initio total-energy calculations using a plane-wave basis set, Phys. Rev. B 54 (1996) 11169–11186, https://doi.org/10.1103/PhysRevB.54.11169.

[32] G. Kresse, J. Furthmüller, Efficiency of ab-initio total energy calculations for metals and semiconductors using a plane-wave basis set, Comput. Mater. Sci. 6 (1996) 15–50, https://doi.org/10.1016/0927-0256(96)00008-0.

[33] G. Kresse, J. Hafner, Ab initio molecular-dynamics simulation of the liquid-metal–amorphous-semiconductor transition in germanium, Phys. Rev. B 49 (1994) 14251–14269, https://doi.org/10.1103/PhysRevB.49.14251.

[34] J.P. Perdew, K. Burke, M. Ernzerhof, Generalized gradient approximation made simple, Phys. Rev. Lett. 77 (1996) 3865–3868, https://doi.org/10.1103/PhysRevLett.77.3865.

[35] P.E. Blöchl, Projector augmented-wave method, Phys. Rev. B 50 (1994) 17953–17979, https://doi.org/10.1103/PhysRevB.50.17953.

[36] H.J. Monkhorst, J.D. Pack, Special points for Brillouin-zone integrations, Phys. Rev. B 13 (1976) 5188–5192, https://doi.org/10.1103/PhysRevB.13.5188.

[37] S.L. Dudarev, G.A. Botton, S.Y. Savrasov, C.J. Humphreys, A.P. Sutton, Electron-energy-loss spectra and the structural stability of nickel oxide: an LSDA+U study, Phys. Rev. B 57 (1998) 1505–1509, https://doi.org/10.1103/PhysRevB.57.1505.

[38] W. Setyawan, S. Curtarolo, High-throughput electronic band structure calculations: challenges and tools, Comput. Mater. Sci. 49 (2010) 299–312, https://doi.org/10.1016/j.commatsci.2010.05.010.

[39] S. Azam, T.V. Vu, D.H. Mirza, M. Irfan, S. Goumri-Said, Effect of Coulomb interactions on optoelectronic properties of Eu doped lanthanide stannates pyrochlore: DFT + U investigations, J. Solid State Chem. 290 (2020) 121522, https://doi.org/10.1016/j.jssc.2020.121522.

[40] K. Momma, F. Izumi, *VESTA 3* for three-dimensional visualization of crystal, volumetric and morphology data, J. Appl. Crystallogr. 44 (2011) 1272–1276, https://doi.org/10.1107/S0021889811038970.

[41] S.J. Clark, M.D. Segall, C.J. Pickard, P.J. Hasnip, M.I.J. Probert, K. Refson, M. C. Payne, First principles methods using CASTEP, Z. für Kristallogr. - Cryst. Mater. 220 (2005) 567–570, https://doi.org/10.1524/zkri.220.5.567.65075.

[42] G.P. Srivastava, D. Weaire, The theory of the cohesive energies of solids, Adv. Phys. 36 (1987) 463–517, https://doi.org/10.1080/00018738700101042.

[43] J.P. Perdew, A. Zunger, Self-interaction correction to density-functional approximations for many-electron systems, Phys. Rev. B 23 (1981) 5048–5079, https://doi.org/10.1103/PhysRevB.23.5048.

[44] D.M. Ceperley, B.J. Alder, Ground state of the electron gas by a stochastic method, Phys. Rev. Lett. 45 (1980) 566–569, https://doi.org/10.1103/PhysRevLett.45.566.

[45] M. Patel, A. Chavda, I. Mukhopadhyay, J. Kim, A. Ray, Nanostructured SnS with inherent anisotropic optical properties for high photoactivity, Nanoscale 8 (2016) 2293–2303, https://doi.org/10.1039/C5NR06731F.
[46] A.V. Malakhovskii, T.V. Kutsak, A.L. Sukhachev, A.S. Aleksandrovsky, A.S. Krylov, I.A. Gudim, M.S. Molokeev, Spectroscopic properties of ErAl3(BO3)4 single crystal, Chem. Phys. 428 (2014) 137–143, https://doi.org/10.1016/j.chemphys.2013.11.008.
[47] Bruker, Bruker AXS TOPAS V4: General Profile and Structure Analysis Software for Powder Diffraction Data, User's Manual. Bruker AXS, Karlsruhe, Germany, 2008.
[48] A.N. Toksumakov, V.S. Baidyshev, D.G. Kvashnin, Z.I. Popov, Bonding duality and optoelectronic properties of bilayer carbon structures based on the T12 phase and penta-graphene, Jetp Lett 117 (2023) 441–448, https://doi.org/10.1134/S0021364023600283.
[49] N.O. Azarapin, A.S. Oreshonkov, I.A. Razumkova, A.S. Aleksandrovsky, N. G. Maximov, I.I. Leonidov, N.P. Shestakov, O.V. Andreev, Evolution of structural, thermal, optical, and vibrational properties of Sc_2S_3, $ScCuS_2$, and $BaScCuS_3$ semiconductors, Eur. J. Inorg. Chem. 2021 (2021) 3355–3366, https://doi.org/10.1002/ejic.202100292.
[50] M.U. Abulkhaev, M.S. Molokeev, A.S. Oreshonkov, A.S. Aleksandrovsky, A. V. Kertman, D.N. Kamaev, O.V. Trofimova, A.V. Elyshev, O.V. Andreev, Properties of GdSF and phase diagram of the GdF3 - Gd2S3 system, J. Solid State Chem. 322 (2023) 123991, https://doi.org/10.1016/j.jssc.2023.123991.
[51] K. Nakamoto Nakamoto, Infrared and Raman Spectra of Inorganic and Coordination Compounds, sixth ed., Wiley, New York, NY, USA, 2009.
[52] E. Cavalli, N. Leonyuk, Comparative investigation on the emission properties of RAl3(BO3)4 (R = Pr, Eu, Tb, Dy, Tm, Yb) crystals with the huntite structure, Crystals 9 (2019) 44, https://doi.org/10.3390/cryst9010044.
[53] K. Binnemans, Interpretation of europium(III) spectra, Coord. Chem. Rev. 295 (2015) 1–45, https://doi.org/10.1016/j.ccr.2015.02.015.
[54] A.S. Aleksandrovsky, V.G. Arkhipkin, L.N. Bezmaternykh, I.A. Gudim, A.S. Krylov, F. Vagizov, Origin of color centers in the flux-grown europium gallium garnet, J. Appl. Phys. 103 (2008) 083102, https://doi.org/10.1063/1.2902365.
[55] M.S. Platunov, I.A. Gudim, E.N. Ovchinnikova, K.A. Kozlovskaya, F. Wilhelm, A. Rogalev, A. Hen, V.Y. Ivanov, A.A. Mukhin, V.E. Dmitrienko, X-Ray natural circular dichroism imaging of multiferroic crystals, Crystals 11 (2021) 531, https://doi.org/10.3390/cryst11050531.